ACS APPLIED MATERIALS & INTERFACES

Research Article

www.acsami.org

Al_2O_3/TiO_2 Nanolaminate Thin Film Encapsulation for Organic Thin Film Transistors via Plasma-Enhanced Atomic Layer Deposition

Lae Ho Kim,[†] Kyunghun Kim,[†] Seonuk Park,[†] Yong Jin Jeong,[†] Haekyoung Kim,[‡] Dae Sung Chung,*[,§] Se Hyun Kim,*[,∥] and Chan Eon Park*[,†]

[†]Polymer Research Institute, Department of Chemical Engineering, Pohang University of Science and Technology, Pohang, North Gyeongsang 790-784, South Korea

[‡]School of Materials Science and Engineering, Yeungnam University, Gyeongsan, North Gyeongsang 712-749, South Korea

[§]School of Chemical Engineering and Material Science, Chung-Ang University, Seoul 156-756, South Korea

[∥]Department of Nano, Medical and Polymer Materials, Yeungnam University, Gyeongsan, North Gyeongsang 712-749, South Korea

S *Supporting Information*

ABSTRACT: Organic electronic devices require a passivation layer that protects the active layers from moisture and oxygen because most organic materials are very sensitive to such gases. Passivation films for the encapsulation of organic electronic devices need excellent stability and mechanical properties. Although Al_2O_3 films obtained with plasma enhanced atomic layer deposition (PEALD) have been tested as passivation layers because of their excellent gas barrier properties, amorphous Al_2O_3 films are significantly corroded by water. In this study, we examined the deformation of PEALD Al_2O_3 films when immersed in water and attempted to fabricate a corrosion-resistant passivation film by using a PEALD-based Al_2O_3/TiO_2 nanolamination (NL) technique. Our Al_2O_3/TiO_2 NL films were found to exhibit excellent water anticorrosion and low gas permeation and require only low-temperature processing (<100 °C). Organic thin film transistors with excellent air-stability (52 days under high humidity (a relative humidity of 90% and a temperature of 38 °C)) were fabricated.

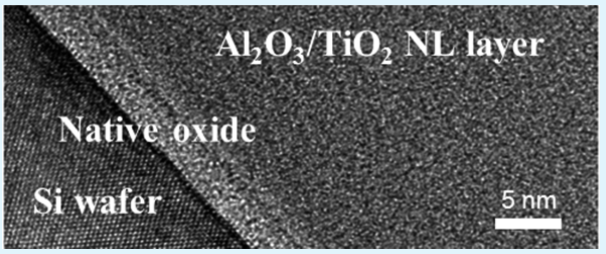

KEYWORDS: *plasma-enhanced atomic layer deposition (PEALD), Al_2O_3, TiO_2, encapsulation, organic thin film transistor (OTFT), nanolamination*

1. INTRODUCTION

Organic electronic devices have attracted considerable attention because of their advantageous properties, including low-cost and simple mass production, as well as their compatibility with flexible substrates.[1] Extensive research has been performed with the goal of commercializing organic electronic devices, i.e., organic thin film transistors (OTFTs), organic light-emitting diodes (OLEDs), and organic photovoltaic cells (OPVs).[2−12] However, the intrinsic vulnerability of organic semiconductor materials to H_2O and O_2 means that an effective permeation barrier is required that can prevent the penetration of these gases into organic devices.[13−16]

Thin film encapsulation, in which a barrier film is directly deposited onto a device, is considered indispensable for flexible electronics and has been performed with various deposition techniques, such as plasma enhanced chemical vapor deposition (PECVD),[17] atomic layer deposition (ALD),[18−20] sputtering,[21] thermal evaporation, inkjet printing,[22] and spin coating processes.[23,24] ALD can produce densely packed, pinhole-free, highly uniform, and conformal films that can act as high quality gas permeation barriers for organic devices. In particular, the plasma-enhanced ALD (PEALD) technique, which provides growth characteristics that are similar to those of typical thermal ALD, enables rapid room temperature deposition by using an O_2 plasma instead of water vapor.[25] Al_2O_3 films deposited with PEALD have been widely investigated as gas permeation barrier films for optoelectronic devices because their barrier properties are excellent even for thicknesses on the scale of a few tens of nanometers.[26] Recently, Jung et al. have reported high quality PEALD-based Al_2O_3 moisture barrier film and shown a low water vapor transmission rate (WVTR) value of 2.6×10^{-4} g m^{-2} day^{-1} at 100 nm thickness.[27] A large number of properties of PEALD-based Al_2O_3 film, such as thermal stability, amorphous structure, and high conformality, can be possible to obtain an excellent gas barrier film.[28] However, amorphous Al_2O_3 films are susceptible to corrosion by water,[29] which means that they are not suitable barriers for conditions of high humidity or water immersion. A new method is therefore required to prevent water corrosion of such films. Abdulagatov et al. have reported the encapsulation of copper with a TiO_2-top and Al_2O_3-bottom bilayer with a total thickness of approximately 20 nm for resistance to water

Received: January 22, 2014
Accepted: April 8, 2014
Published: April 8, 2014

   dx.doi.org/10.1021/am500458d | ACS Appl. Mater. Interfaces 2014, 6, 6731−6738

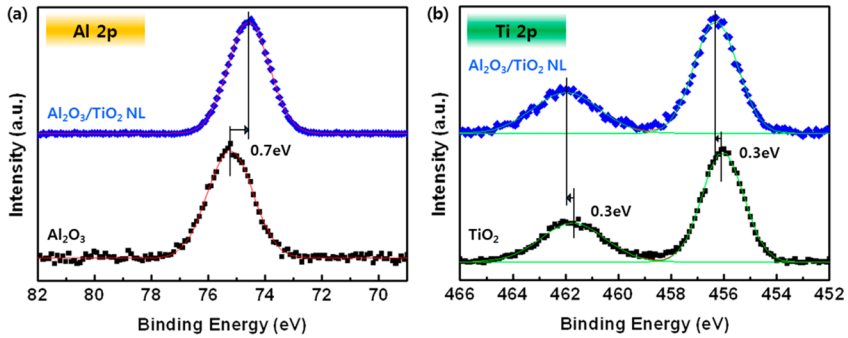

Figure 1. X-ray photoemission (XPS) spectra of single Al_2O_3 and TiO_2, as well as Al_2O_3/TiO_2 NL films for (a) Al 2p and (b) Ti 2p core levels.

corrosion by using thermal ALD.[29] TiO_2 is known to display good resistance to water corrosion, and the combination of TiO_2 and Al_2O_3 was found to prevent water corrosion at the barrier surface and to protect the copper layer in water. However, a TiO_2/Al_2O_3 bilayer structure is not the best strategy for the long-term stability of passivation films with respect to water corrosion, because TiO_2 is not an effective gas barrier and thus could allow water molecules to diffuse into the Al_2O_3 layer.

In the present study, we aimed to prepare Al_2O_3/TiO_2 nanolaminate (NL) films consisting of alternately stacked atomic sublayers with excellent water anticorrosion, low gas permeation, and low-temperature processing. Recently, several researchers have attempted to prepare NL films with various functionalities by using ALD processes.[30,31] However, further studies are still required to optimize the processing of such films with respect to their applications in optoelectronic organic devices. In addition, well-controlled Al_2O_3/TiO_2 NL films have not previously been fabricated with PEALD. We determined the structural characteristics of the Al_2O_3/TiO_2 NL films and investigated the physical properties of the films as barriers to water corrosion and gas permeation. In particular, the 50 nm thick nanolaminate films were used in OTFTs as encapsulation layers, and then, the reliabilities of the devices were evaluated as functions of time upon exposure to high humidity air.

2. EXPERIMENTAL SECTION

Al_2O_3 and Al_2O_3/TiO_2 NL Film Preparation and Characterization. Al_2O_3 and Al_2O_3/TiO_2 NL films were deposited on either a Si (100) wafer or a p-type pentacene-based OTFT by using PEALD (LTSR-150, Leintech). The Si wafer was used to investigate the chemical and physical properties of the oxide films. The Si wafer was washed with acetone and then isopropyl alcohol in an ultrasonic bath for 20 min and then dried with a N_2 blower. In order to remove any dust and to obtain a hydroxyl-rich surface before the PEALD process, the Si wafer substrate was exposed to UV radiation for 10 min.

The precursor used in the PEALD of the Al_2O_3 films was trimethylaluminum (TMA, Lake LED Materials), and for the Al_2O_3/TiO_2 NL films, both TMA and tetrakis(dimethylamino)-titanium (TDMAT, EG Chem) were used. TMA and TDMAT were injected into the reaction chamber without a carrier gas. O_2 plasma was used as the oxygen source, and the PEALD substrate heater was operated at a constant temperature of 100 °C. All samples were placed onto the PEALD substrate for 30 min before deposition to thermal equilibrium between samples and the ALD substrate. The temperature of the TMA source was maintained at room temperature, and the base pressure and processing pressure inside the reactor were 0.01 and 0.5 Torr, respectively. The sequence of pulses for one cycle deposition of an Al_2O_3 film was as follows: TMA feeding (0.1 s), Ar purging (10 s), O_2 feeding (1.5 s), O_2 feeding with 200 W RF plasma power (3 s), and Ar purging (5 s).

The temperature of the TDMAT source was maintained at 60 °C with a heating system because of its low vapor pressure at room temperature, and the base pressure and processing pressure inside the reactor were retained at levels identical to those used in the Al_2O_3 film deposition process. The sequence of pulses for one cycle deposition of an Al_2O_3/TiO_2 NL film was as follows: TMA feeding (0.1 s), Ar purging (10 s), O_2 feeding (1.5 s), O_2 feeding with 200 W RF plasma power (3 s), and Ar purging (5 s) for Al_2O_3 monolayer deposition and then TDMAT feeding (1 s), Ar purging (10 s), O_2 feeding (1.5 s), O_2 feeding with 100 W RF plasma power (3 s), and Ar purging (10 s) for TiO_2 monolayer deposition.

The thicknesses of the films were measured by using a spectroscopic ellipsometer (J.A. Woollam, M-2000). To investigate the structural characteristics, chemical compositions, and morphologies of the deposited films, we used X-ray photoelectron spectroscopy (XPS, 4D beamline at the Pohang Accelerator Laboratory in Korea), atomic force microscopy (AFM, VEECO Dimension 3100), scanning electron microscopy (SEM, JEOL JSM-7401F), and high resolution transmission electron microscopy (HR-TEM, JEOL JEM-2100F). The water vapor transmission rate (WVTR) values were measured by performing calcium tests.

OTFT Fabrication and Passivation. A 30 nm layer of ethylene-norborene cyclic olefin copolymer (Polyscience) was spin-coated onto a precleaned n-type Si (100) wafer covered with a 100 nm layer of SiO_2 as a gate dielectric and insulator to provide a high performance bilayer gate dielectric for the OTFTs.[32] The samples were heated on a 120 °C hot plate for 30 min to remove any residual solvent. Subsequently, a 50 nm pentacene layer was patterned through a shadow mask by evaporation to form an organic semiconductor layer with an organic molecular beam deposition (OMBD) system. A 50 nm thick gold layer was added to the pentacene layer by using a vacuum thermal evaporator with a deposition rate of 3 Å s^{-1} and vacuum conditions of 10^{-5} Torr to provide the source/drain electrodes. The channel length (L) and width (W) of the shadow mask used in gold deposition were fixed at 100 and 1500 μm, respectively. Then, a 200 nm silicon monoxide (SiO) layer was deposited onto the OTFTs in an evaporation chamber (SUNIC SUNICEL 0603) under a 10^{-5} Torr vacuum as a buffer layer to prevent any plasma damage during the PEALD process.[33] 50 nm Al_2O_3 or Al_2O_3/TiO_2 NL films were deposited with the method discussed above onto the prepared OTFT devices as passivation layers.

Device Characterization. The electrical properties of the OTFTs were characterized by using a home-built combination of Keithley 2400 and 236 source/measure units. The field effect mobilities (μ) of the OTFTs were calculated from the slopes of plots of the square-root of the drain current ($I_D^{1/2}$) versus the gate voltage (V_G). The long-term stabilities of the OTFTs were tested by storing them at 38 °C in a 90% relative humidity (RH) conditioned environmental chamber. The electrical characteristics were measured as a function of time.

3. RESULTS AND DISCUSSION

Chemical and Physical Properties of the Al_2O_3/TiO_2 NL Films. The chemical composition of the Al_2O_3/TiO_2

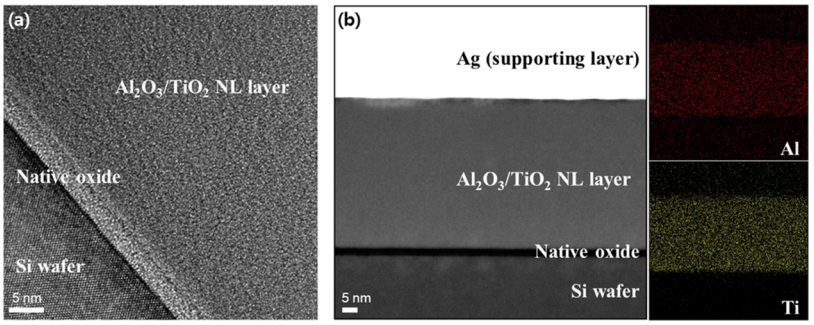

Figure 2. (a) Cross-sectional TEM and (b) TEM-EDS mapping images showing amorphous structure of Al_2O_3/TiO_2 NL film without any interfaces.

interface was investigated in detail with XPS. Each NL film consists of 12 alternating layers of Al_2O_3 and TiO_2 on a Si substrate; each layer was prepared in a single PEALD deposition cycle. The nominal thicknesses of the Al_2O_3 and TiO_2 layers were finely controlled on the atomic scale during the processing, with values of 1.8 and 0.75 Å, respectively. In addition, to avoid charging effects during the XPS measurements, the film thicknesses of the samples investigated here vary by less than 3 nm. Figure 1 shows the Al 2p and Ti 2p core level spectra for single Al_2O_3 and TiO_2 films and for a Al_2O_3/TiO_2 NL film. The core level peaks of neat Al_2O_3 and TiO_2 (the black square dotted lines at the bottom of the figure panels) are at 75.2 eV (Al 2p), 461.7 eV (Ti 2p 1/2), and 456.0 eV (Ti 2p 3/2), which is in agreement with the binding energy reported for Al_2O_3 and TiO_2.[34] In the case of the Al_2O_3/TiO_2 NL film, the Al 2p core level is shifted toward a lower binding energy (74.5 eV) and the Ti 2p core level is shifted toward a higher binding energy (462.0 eV for Ti 2p 1/2 and 456.3 eV for Ti 2p 3/2) relative to the reference peaks mentioned above. The electro-negativities of Al (1.61) and Ti (1.54) mean that Al and Ti tend to attract and donate electrons, respectively. Therefore, the observed core level shifts for Al and Ti could result from Al−O−Ti bonding processes between the Al_2O_3 and TiO_2 atomic sublayers. Similar core level shifts in a Al_2O_3/ZrO_2 NL film prepared in a thermal ALD system have recently been reported.[30] The formation of thermodynamically stable bonds between Al_2O_3 and ZrO_2 results in shifts in the Al 2p and Zr 3d core levels toward lower and higher binding energies, respectively, as is in accord with their electro-negativities (Al: 1.61 and Zr: 1.33).[30]

In order to characterize the overall morphology of the Al_2O_3/TiO_2 NL films, cross-sectional TEM-EDS were carried out on 50 nm thick NL films grown on a Si wafer. The films were prepared by using 196 cycles of PEALD deposition at 100 °C, and the growth rate of the Al_2O_3/TiO_2 NL films was approximately 2.55 Å/cycle, which means that the nominal thicknesses of the layers deposited during one cycle were 1.8 Å (Al_2O_3) and 0.75 Å (TiO_2). In the cross-sectional TEM and EDS images (Figure 2), it can be seen that Al and Ti atoms are uniformly distributed over the NL film with no significant phase separation or crystallites (see the Supporting Information Figure S1, XRD spectrum clearly shows that PEALD-based NL film has full amorphous morphology). In spite of the sequential deposition of Al_2O_3 and TiO_2, the atomic-scale thicknesses of the layers result in the emergence of an amorphous alloy-type film morphology, instead of a simple multistacked morphology. Grain boundaries arising from polycrystalline structure as well as interfaces between heterogeneous layers can act as permeation pathways for gases, thereby deteriorating the passivation efficiency of the film and limiting its effectiveness as a gas barrier.

Figure 3 shows the leakage current density versus electrical field characteristics measured using the device configuration

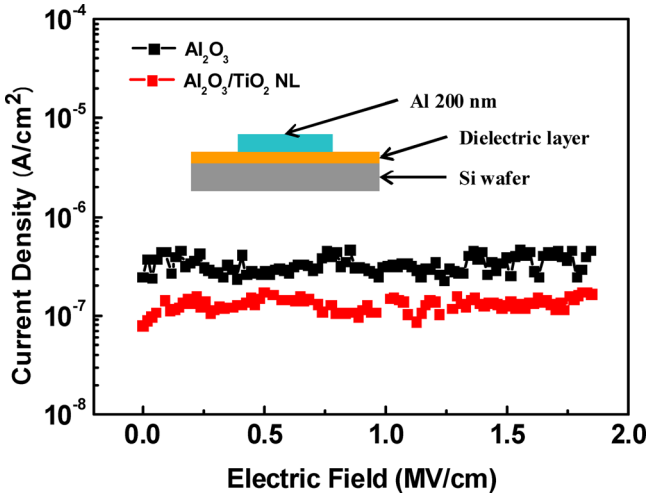

Figure 3. Breakdown voltages of single Al_2O_3 and Al_2O_3/TiO_2 NL dielectric layers. The inset shows a schematic image of the breakdown voltage measurement setup.

shown in the inset. Single Al_2O_3 and Al_2O_3/TiO_2 NL films were interposed between a heavily doped Si wafer and a 200 nm Al electrode. Although the breakdown of the two samples did not occur within the measured electric field range (up to 1.8 MV cm^{-1}), the leakage current density of the NL sample (1.18×10^{-7} A cm^2) is approximately 2.5 times lower than that of the Al_2O_3 film (3.34×10^{-7} A cm^2). Generally, a lower leakage current density is related to an increase in film density and a decrease in the number of voids or defects in the film. These results confirm that our nanolamination method can produce densely packed films.

Gas Permeation Barrier and Water-Resistance Properties of the PEALD Films. Figures 4 and 5 show FE-SEM and AFM images, respectively, of the surface of the single Al_2O_3 and Al_2O_3/TiO_2 NL films before and after immersion in water at 90 °C. Both films were deposited at 100 °C with a thickness of approximately 50 nm. Before water immersion, the Al_2O_3 film has a very smooth and clean surface (the 10 nm spurs on the surface in Figure 5 are platinum grains that were deposited onto the sample surfaces to enhance the focus of the FE-SEM). However, after only a 30 min immersion in water at 90 °C, the surface roughness increases and petal structures are formed (see Figures 4b and 5b) that have been referred to as

dx.doi.org/10.1021/am500458d | ACS Appl. Mater. Interfaces 2014, 6, 6731−6738

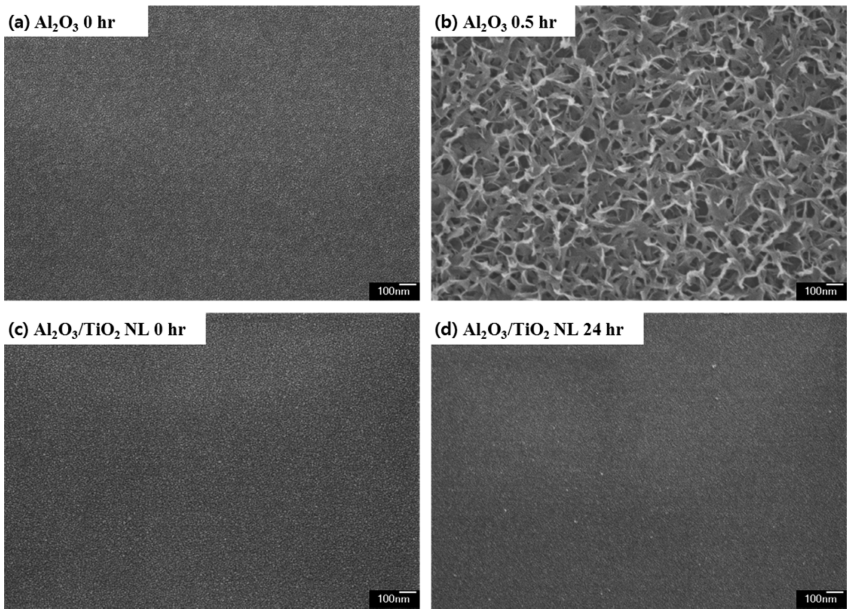

Figure 4. FE-SEM photographs for the surface of single Al_2O_3 and Al_2O_3/TiO_2 NL films (a, c) before and (b, d) after immersion in water at 90 °C.

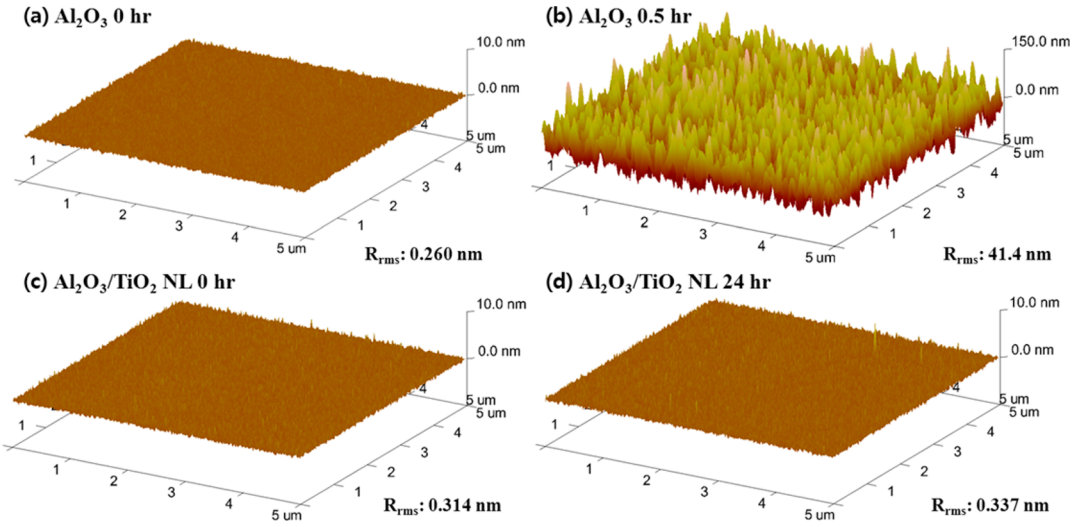

Figure 5. AFM images for the surface of single Al_2O_3 and Al_2O_3/TiO_2 NL films (a, c) before and (b, d) after immersion in water at 90 °C.

"flowerlike" structures.[35] Such destruction of the Al_2O_3 surface could be due to the corrosion of Al_2O_3 by water as described in chemical reactions 1 and 2,[36] which implies that prolonged exposure to moisture at room temperature can produce the barrier failure of the Al_2O_3 film (see the Supporting Information Figure S2 for film thickness and refractive index change by immersion time of single Al_2O_3 and Al_2O_3/TiO_2 NL films at room temperature).

$$Al_2O_3(s) + 6H^+(aq) + 3H_2O(l) \rightarrow 2[Al(H_2O)_3]^{3+}(aq) \quad (1)$$

$$Al_2O_3(s) + 2OH^-(aq) + 3H_2O(l) \rightarrow 2[Al(OH)_4]^-(aq) \quad (2)$$

In contrast, there is no significant change in the Al_2O_3/TiO_2 NL films even after the long immersion time of 24 h, as shown in Figures 4d and 5d. In addition, the Al_2O_3/TiO_2 NL films have better gas permeation barrier properties than the single Al_2O_3 and TiO_2 films. Figure 6 shows the plots obtained from the calcium corrosion tests, which were used to obtain the WVTR values of single Al_2O_3 and TiO_2 films and a Al_2O_3/TiO_2 NL film; the results are summarized in Table 1. All oxide films were deposited with a thickness of 50 nm on 200 μm PEN (polyethylene naphthalate) by means of PEALD. In the calcium corrosion test, 120 nm thick aluminum was deposited on glass substrates as electrodes in order to measure the conductance of the calcium during oxidation by water. Then, a 250 nm thick calcium layer (20 × 20 mm^2) was deposited on the glass in partial overlap with the aluminum layer. Finally, calcium-deposited glass was encapsulated by barrier-coated PEN film with UV-cured sealant (Figure 6a). The WVTR values were calculated with the following equation:[37]

$$\mathrm{WVTR} = -n\cdot(M_{H_2O}/M_{Ca})\cdot\rho_{Ca}\cdot\sigma\cdot[d(1/R)/dt]\cdot(S_{Ca}/S)$$

where n is the molar equivalent of the degradation reaction. M_{H_2O} and M_{Ca} are the molecular weights of H_2O and calcium, respectively, and ρ_{Ca} and σ are the density and resistivity of the calcium, respectively. S_{Ca} is the area of calcium, and S is the

dx.doi.org/10.1021/am500458d | ACS Appl. Mater. Interfaces 2014, 6, 6731−6738

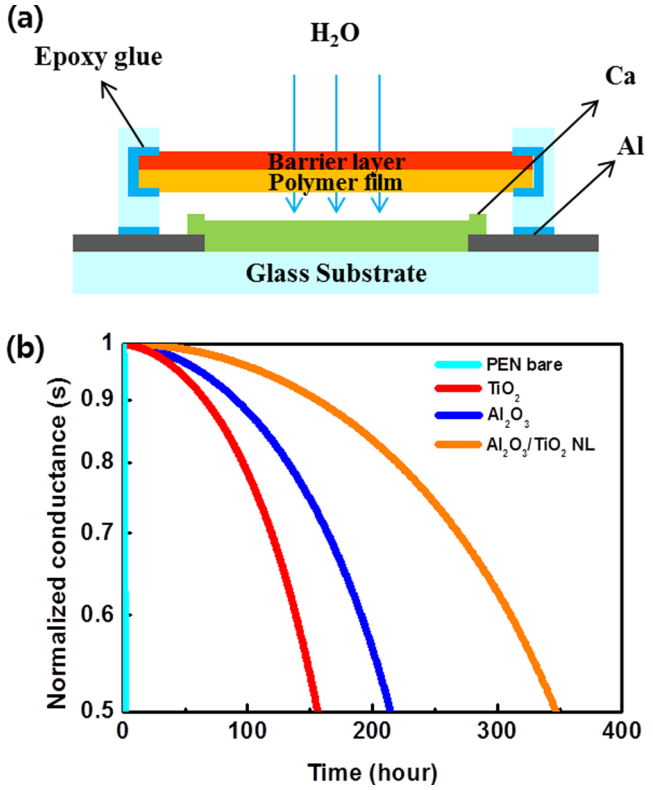

Figure 6. (a) Overall test-bed scheme of the calcium corrosion test. (b) Normalized conductance of single Al_2O_3 and TiO_2, as well as Al_2O_3/TiO_2 NL barrier film at 60 °C 90% RH condition.

transmission area of the water vapor. The rate of change in the conductance, $d(1/R)/dt$, can be extracted from the slope of the calcium test plot. As shown in Figure 6b, the calcium corrosion rates gradually decrease and the WVTR values in Table 1 also decrease in the following order: single TiO_2 ($6.32 \times 10^{-4} \pm 2.04 \times 10^{-5}$ g m^{-2} day^{-1}), Al_2O_3 ($3.75 \times 10^{-4} \pm 3.51 \times 10^{-5}$ g m^{-2} day^{-1}), and Al_2O_3/TiO_2 NL ($1.81 \times 10^{-4} \pm 8.64 \times 10^{-5}$ g m^{-2} day^{-1}).

The effectiveness of the passivation provided by the NL films (such as water anticorrosion and the lowest WVTR value) is due to two main factors: the dense film morphology and the introduction of TiO_2 into the Al_2O_3 backbone. In general, defects in oxide films facilitate the formation of hydroxyl groups, which increase the solubility of the films in water and offer pathways for gas diffusion. In addition, tight Al−O−Ti bond formation might decrease the hydrolysis of the Al_2O_3 bond in water.[38,39]

Characteristics of an OTFT Device Passivated with an Al_2O_3/TiO_2 NL Film. A 50 nm thick single Al_2O_3 film and an Al_2O_3/TiO_2 NL film were each applied to pentacene-based OTFTs, and the air-stabilities of the resulting devices were evaluated in high humidity air. The investigated OTFTs were fabricated on 100 nm thick thermally grown SiO_2/Si substrates, with bottom-gate and top-contact device architecture, as shown in Figure 7a. Hydrophobic ethylene-norborene copolymer (COC) was spin-cast onto the SiO_2 dielectrics to enhance the

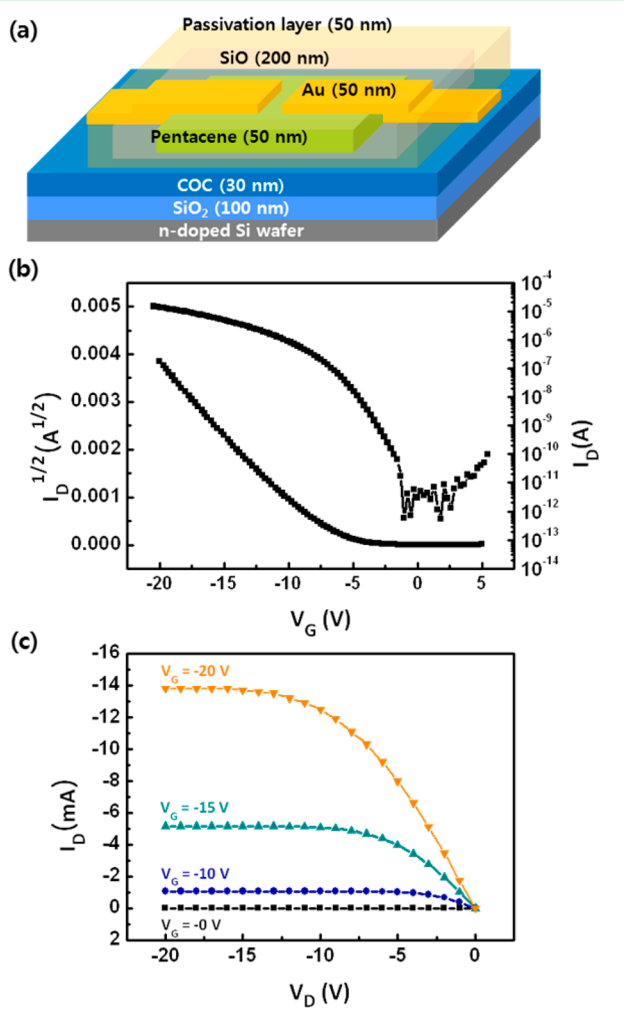

Figure 7. (a) Schematic diagrams of pentacene-based OTFT with COC-SiO_2 bilayer gate dielectric. (b) Transfer and (c) output characteristics of as-fabricated OTFT device.

growth of the pentacene films and to minimize the number of interface trap states due to surface hydroxyl groups. Prior to the PEALD of the Al_2O_3 and Al_2O_3/TiO_2 NL films, 200 nm thick silicon monoxide layers were deposited onto the OTFT devices by performing thermal evaporation to protect them from plasma damage during PEALD.[13,33]

The field-effect mobilities (μ_{FET}) of the OTFTs were obtained from the slopes of plots of the square root of the drain current (I_D) versus the gate voltage (V_G) in the saturation current region by using the equation: $I_D = (WC_i/2L)\mu(V_G - V_{th})^2$,[40] where I_D is the drain current and C_i is the capacitance per unit area of the dielectric, which for our COC/SiO_2 dielectrics is approximately 10 nF cm^{-2}. The initial average μ_{FET} and the threshold voltage (V_{th}) for the OTFT devices

Table 1. Water Vapor Transmission Rate (WVTR) Values of PEN Bare and 50 nm Thick Al_2O_3, TiO_2, and Al_2O_3/TiO_2 NL Passivated PEN Film

passivation materials	PEN bare	TiO_2	Al_2O_3	Al_2O_3/TiO_2 NL
WVTR (g m^{-2} day^{-1})	5.18×10^{-1} $\pm 3.26 \times 10^{-2}$	6.32×10^{-4} $\pm 2.04 \times 10^{-5}$	3.75×10^{-4} $\pm 3.51 \times 10^{-5}$	1.81×10^{-4} $\pm 8.64 \times 10^{-5}$

dx.doi.org/10.1021/am500458d | ACS Appl. Mater. Interfaces 2014, 6, 6731−6738

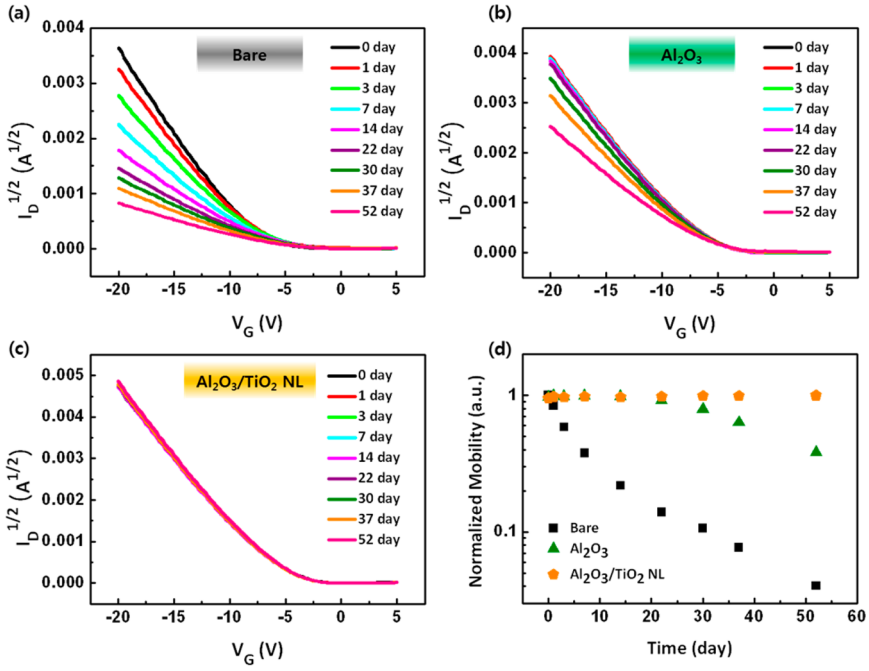

Figure 8. Time-dependent $I_D^{1/2}$ versus V_G characteristics of (a) bare and (b) 50 nm Al_2O_3 and (c) 50 nm Al_2O_3/TiO_2 NL film passivated OTFTs. (d) Time-dependent field-effect mobilities of PEALD films.

were 0.610 cm^2 V^{-1} s^{-1} and −7.61 V, respectively. The air stabilities of the pentacene OTFT devices passivated with single Al_2O_3 and Al_2O_3/TiO_2 NL films were investigated by performing time-dependent electrical performance measurements in a chamber under constant environmental conditions: 38 °C, 90% RH, and dark. The unpassivated pentacene OTFT was also stored in the same environmental chamber as a reference device.

Figure 8 shows the time-dependent $I_D^{1/2}$ versus V_G characteristics of the pentacene OTFTs, one as-fabricated, and the devices with two types of passivation (see the Supporting Information Figure S3 for time-dependent device characteristics only with SiO layer OTFT). The evolutions of the normalized μ_{FET} values for the corresponding devices are summarized in Figure 8d. As shown in Figure 8a, there is a dramatic reduction in the maximum drain current of the unpassivated device, with a shift in V_{th} in the negative V_G direction after 52 days of measurement. Water molecules that diffuse into the pentacene film are likely to degrade the device performance by interacting with pentacene molecules and forming traps at the grain boundaries, thereby reducing μ_{FET} and the on-current.[41−44] In contrast, the device performance of the OTFT passivated with a single Al_2O_3 film was maintained for 22 days; μ_{FET} and V_{th} degrade with time. The corrosion of Al_2O_3 films in humid air will be slower than when they are immersed in hot water, so the passivation layer will protect the device from the air during the early stages of the air-stability measurements. However, long-term exposure to humid air is likely to result in the destruction of the Al_2O_3 passivation film due to its water-corrosion behavior (see Figure 9c), thereby leading to the degradation of device performance. In contrast to the other samples, the OTFT device passivated with an Al_2O_3/TiO_2 NL film was found to exhibit excellent air-stability even after prolonged exposure to humid air, as expected (Figures 8c and 9d).

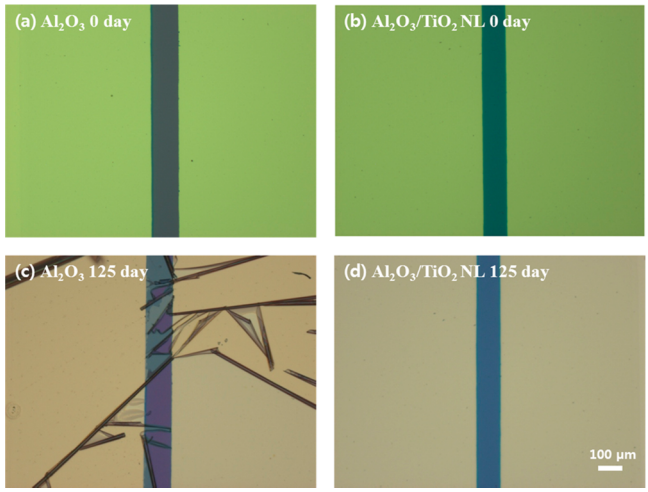

Figure 9. Optical microscopy images of the channel regions of OTFTs passivated with single Al_2O_3 and Al_2O_3/TiO_2 NL film (a, b) before and (c, d) after 125 day storage in 38 °C 90% RH chamber.

4. CONCLUSION

In summary, Al_2O_3/TiO_2 nanolaminated films were tested as passivation layers for OTFT devices. Each Al_2O_3/TiO_2 NL film has a very smooth surface and exhibits a large breakdown field, water anticorrosion, and very low WVTR values, which are superior to those of the other investigated passivation films: PEALD-based single Al_2O_3 and TiO_2 films. The OTFT passivated with an Al_2O_3/TiO_2 NL film (50 nm) was found to have a prolonged lifetime exceeding 52 days. Therefore, the water-resistant Al_2O_3/TiO_2 NL film coating has great potential for practical applications, particularly as a capping material for OPVs, OLEDs, and OTFTs.

dx.doi.org/10.1021/am500458d | ACS Appl. Mater. Interfaces 2014, 6, 6731−6738

■ ASSOCIATED CONTENT

Supporting Information

The out-of-plane XRD spectrum of 50 nm thick Al_2O_3/TiO_2 NL film, film thickness, and refractive index on Si wafer versus time in water at room temperature for single Al_2O_3 and Al_2O_3/TiO_2 NL coatings, and time-dependent $I_D^{1/2}$ versus V_G characteristics of 200 nm thick SiO film passivated OTFT. This material is available free of charge via the Internet at http://pubs.acs.org.

■ AUTHOR INFORMATION

Corresponding Authors

*E-mail: cep@postech.ac.kr. Fax: +82-54-279-8298. Tel: +82-54-279-2269.

*E-mail: shkim97@yu.ac.kr. Fax: +82-53-810-4686. Tel: +82-53-810-2779.

*E-mail: dchung@cau.ac.kr. Fax: +82-53-810-4686. Tel: +82-53-810-2779.

Notes

The authors declare no competing financial interest.

■ ACKNOWLEDGMENTS

This work was supported by the New & Renewable Energy of the Korea Institute of Energy Technology Evaluation and Planning (KETEP) grant funded by the Korea government Ministry of Knowledge Economy (No. 20123010010140), the Center for Advanced Soft-Electronics funded by the Ministry of Science, ICT and Future Planning as Global Frontier Project (2011-0031639), and a National Research Foundation of Korea (NRF) grant funded by the Korean government (MSIP) (NRF-2011-357-D00057).

■ REFERENCES

(1) Forrest, S. R. The Path to Ubiquitous and Low-Cost Organic Electronic Appliances on Plastic. *Nature* **2004**, *428*, 911−918.

(2) Yang, S.; Hwang, C.-S.; Lee, J.-I.; Yoon, S.-M.; Ryu, M.-K.; Cho, K.-I.; Park, S.-H. K.; Kim, S.-H.; Park, C.-E.; Jang, J. Water-Related Abnormal Instability of Transparent Oxide/Organic Hybrid Thin Film Transistors. *Appl. Phys. Lett.* **2011**, *98*, 103515.

(3) Kim, S. H.; Jang, M.; Yang, H.; Anthony, J. E.; Park, C. E. Physicochemically Stable Polymer-Coupled Oxide Dielectrics for Multipurpose Organic Electronic Applications. *Adv. Funct. Mater.* **2011**, *21*, 2198−2207.

(4) Halik, M.; Klauk, H.; Zschieschang, U.; Schmid, G.; Dehem, C.; Schutz, M.; Maisch, S.; Effenberger, F.; Brunnbauer, M.; Stellacci, F. Low-Voltage Organic Transistors with an Amorphous Molecular Gate Dielectric. *Nature* **2004**, *431*, 963−966.

(5) Klauk, H. Organic Thin-Film Transistors. *Chem. Soc. Rev.* **2010**, *39*, 2643−2666.

(6) Xiao, L.; Chen, Z.; Qu, B.; Luo, J.; Kong, S.; Gong, Q.; Kido, J. Recent Progresses on Materials for Electrophosphorescent Organic Light-Emitting Devices. *Adv. Mater.* **2011**, *23*, 926−952.

(7) Gather, M. C.; Köhnen, A.; Meerholz, K. White Organic Light-Emitting Diodes. *Adv. Mater.* **2011**, *23*, 233−248.

(8) Han, T.-H.; Lee, Y.; Choi, M.-R.; Woo, S.-H.; Bae, S.-H.; Hong, B. H.; Ahn, J.-H.; Lee, T.-W. Extremely Efficient Flexible Organic Light-Emitting Diodes with Modified Graphene Anode. *Nat. Photonics* **2012**, *6*, 105−110.

(9) Geffroy, B.; le Roy, P.; Prat, C. Organic Light-Emitting Diode (OLED) Technology: Materials, Devices and Display Technologies. *Polym. Int.* **2006**, *55*, 572−582.

(10) Ameri, T.; Dennler, G.; Lungenschmied, C.; Brabec, C. J. Organic Tandem Solar Cells: A Review. *Energy Environ. Sci.* **2009**, *2*, 347−363.

(11) Grätzel, M. Photoelectrochemical Cells. *Nature* **2001**, *414*, 338−344.

(12) Kelley, T. W.; Baude, P. F.; Gerlach, C.; Ender, D. E.; Muyres, D.; Haase, M. A.; Vogel, D. E.; Theiss, S. D. Recent Progress in Organic Electronics: Materials, Devices, and Processes. *Chem. Mater.* **2004**, *16*, 4413−4422.

(13) Kim, S. H.; Yoon, W. M.; Jang, M.; Yang, H.; Park, J.-J.; Park, C. E. Damage-Free Hybrid Encapsulation of Organic Field-Effect Transistors to Reduce Environmental Instability. *J. Mater. Chem.* **2012**, *22*, 7731−7738.

(14) Schaer, M.; Nüesch, F.; Berner, D.; Leo, W.; Zuppiroli, L. Water Vapor and Oxygen Degradation Mechanisms in Organic Light Emitting Diodes. *Adv. Funct. Mater.* **2001**, *11*, 116−121.

(15) Potscavage, W. J.; Yoo, S.; Domercq, B.; Kippelen, B. Encapsulation of Pentacene/C_{60} Organic Solar Cells with Al_2O_3 Deposited by Atomic Layer Deposition. *Appl. Phys. Lett.* **2007**, *90*, 253511.

(16) Jørgensen, M.; Norrman, K.; Krebs, F. C. Stability/Degradation of Polymer Solar Cells. *Sol. Energy Mater. Sol. Cells* **2008**, *92*, 686−714.

(17) Kim, H.-K.; Kim, M. S.; Kang, J.-W.; Kim, J.-J.; Yi, M.-S. High-Quality Thin-Film Passivation by Catalyzer-Enhanced Chemical Vapor Deposition for Organic Light-Emitting Diodes. *Appl. Phys. Lett.* **2007**, *90*, 013502.

(18) Jeon, H.; Shin, K.; Yang, C.; Park, C. E.; Park, S. -H. K. Thin-Film Passivation by Atomic Layer Deposition for Organic Field-Effect Transistors. *Appl. Phys. Lett.* **2008**, *93*, 163304.

(19) Meyer, J.; Görrn, P.; Bertram, F.; Hamwi, S.; Winkler, T.; Johannes, H.-H.; Weimann, T.; Hinze, P.; Riedl, T.; Kowalsky, W. Al_2O_3/ZrO_2 Nanolaminates as Ultrahigh Gas-Diffusion Barriers—A Strategy for Reliable Encapsulation of Organic Electronics. *Adv. Mater.* **2009**, *21*, 1845−1849.

(20) Dameron, A. A.; Davidson, S. D.; Burton, B. B.; Carcia, P. F.; McLean, R. C.; George, S. M. Gas Diffusion Barriers on Polymers Using Multilayers Fabricated by Al_2O_3 and Rapid SiO_2 Atomic Layer Deposition. *J. Phys. Chem. C* **2008**, *112*, 4573−4580.

(21) Sugimoto, A.; Ochi, H.; Fujimura, S.; Yoshida, A.; Miyadera, T.; Tsuchida, M. Flexible OLED Displays Using Plastic Substrates. *IEEE J. Sel. Top. Quantum Electron.* **2004**, *10*, 107−114.

(22) Nam, S.; Jeon, H.; Kim, S. H.; Jang, J.; Yang, C.; Park, C. E. An Inkjet-Printed Passivation Layer Based on a Photocrosslinkable Polymer for Long-Term Stable Pentacene Field-Effect Transistors. *Org. Electron.* **2009**, *10*, 67−72.

(23) Nam, S.; Jang, J.; Kim, K.; Yun, W. M.; Chung, D. S.; Hwang, J.; Kwon, O. K.; Chang, T.; Park, C. E. Solvent-Free Solution Processed Passivation Layer for Improved Long-Term Stability of Organic Field-Effect Transistors. *J. Mater. Chem.* **2011**, *21*, 775−780.

(24) Cho, S.; Lee, K.; Heeger, A. J. Extended Lifetime of Organic Field-Effect Transistors Encapsulated with Titanium Sub-Oxide as an "Active" Passivation/Barrier Layer. *Adv. Mater.* **2009**, *21*, 1941−1944.

(25) Groner, M. D.; Fabreguette, F. H.; Elam, J. W.; George, S. M. Low-Temperature Al_2O_3 Atomic Layer Deposition. *Chem. Mater.* **2004**, *16*, 639−645.

(26) Langereis, E.; Creatore, M.; Heil, S. B. S.; van de Sanden, M. C. M.; Kessels, W. M. M. Plasma-Assisted Atomic Layer Deposition of Al_2O_3 Moisture Permeation Barriers on Polymers. *Appl. Phys. Lett.* **2006**, *89*, 081915.

(27) Jung, H.; Choi, H.; Jeon, H.; Lee, S.; Jeon, H. Radio Frequency Plasma Power Dependence of the Moisture Permeation Barrier Characteristics of Al_2O_3 Films Deposited by Remote Plasma Atomic Layer Deposition. *J. Appl. Phys.* **2013**, *114*, 173511.

(28) Jakschik, S.; Schroeder, U.; Hecht, T.; Gutsche, M.; Seidl, H.; Bartha, J. W. Crystallization Behavior of Thin ALD-Al_2O_3 Films. *Thin Solid Films* **2003**, *425*, 216−220.

(29) Abdulagatov, A. I.; Yan, Y.; Cooper, J. R.; Zhang, Y.; Gibbs, Z. M.; Cavanagh, A. S.; Yang, R. G.; Lee, Y. C.; George, S. M. Al_2O_3 and TiO_2 Atomic Layer Deposition on Copper for Water Corrosion Resistance. *ACS Appl. Mater. Interfaces* **2011**, *3*, 4593−4601.

(30) Meyer, J.; Schmidt, H.; Kowalsky, W.; Riedl, T.; Kahn, A. The Origin of Low Water Vapor Transmission Rates through Al_2O_3/ZrO_2

Nanolaminate Gas-Diffusion Barriers Grown by Atomic Layer Deposition. *Appl. Phys. Lett.* **2010**, *96*, 243308.
(31) Meyer, J.; Schneidenbach, D.; Winkler, T.; Hamwi, S.; Weimann, T. Reliable Thin Film Encapsulation for Organic Light Emitting Diodes Grown by Low-Temperature Atomic Layer Deposition. *Appl. Phys. Lett.* **2009**, *94*, 233305.
(32) Jang, J.; Nam, S.; Yun, W. M.; Yang, C.; Hwang, J.; An, T. K.; Chung, D. S.; Park, C. E. High T_g Cyclic Olefin Copolymer/Al_2O_3 Bilayer Gate Dielectrics for Flexible Organic Complementary Circuits with Low-Voltage and Air-Stable Operation. *J. Mater. Chem.* **2011**, *21*, 12542−12546.
(33) Yun, W. M.; Jang, J.; Nam, S.; Kim, L. H.; Seo, S. J.; Park, C. E. Thermally Evaporated SiO Thin Films as a Versatile Interlayer for Plasma-Based OLED Passivation. *ACS Appl. Mater. Interfaces* **2012**, *4*, 3247−3253.
(34) Vitanov, P.; Harizanova, A.; Angelov, C.; Petrov, I.; Alexieva, Z.; Stefanov, P. Structure and Optical Properties of $(Al_2O_3)_x(TiO)_{1-x}$ Thin Films Prepared by a Sol−Gel Processing. *Vacuum* **2004**, *76*, 215−218.
(35) Tadanaga, K.; Katata, N.; Minami, T. Super-Water-Repellent Al_2O_3 Coating Films with High Transparency. *J. Am. Ceram. Soc.* **1997**, *80*, 1040−1042.
(36) Pasieczna-Patkowska, S.; Ryczkowski, J. Spectroscopic Studies of Alumina Supported Nickel Catalysts Precursors: Part II - Catalysts Prepared from Alkaline Solutions. *Ann. UMCS, Chem.* **2010**, *65*, 121−131.
(37) Han, Y. C.; Jang, C.; Kim, K. J.; Choi, K. C.; Jung, K.; Bae, B.-S. The Encapsulation of an Organic Light-Emitting Diode Using Organic−Inorganic Hybrid Materials and MgO. *Org. Electron.* **2011**, *12*, 609−613.
(38) Luo, Y. R. *Comprehensive Handbook of Chemical Bond Energies*; Taylor and Francis Group: Boca Raton, FL, 2007.
(39) Su, Z.; Zhou, W. Formation Mechanism of Porous Anodic Aluminium and Titanium Oxides. *Adv. Mater.* **2008**, *20*, 3663−3667.
(40) Wen, Y.; Liu, Y.; Di, C.; Wang, Y.; Sun, X.; Guo, Y.; Zheng, J.; Wu, W.; Ye, S.; Yu, G. Improvements in Stability and Performance of N,N′-Dialkyl Perylene Diimide-Based N-Type Thin-Film Transistors. *Adv. Mater.* **2009**, *21*, 1631−1635.
(41) Qiu, Y.; Hu, Y.; Dong, G.; Wang, L.; Xie, J.; Ma, Y. H_2O Effect on the Stability of Organic Thin-Film Field-Effect Transistors. *Appl. Phys. Lett.* **2003**, *83*, 1644−1646.
(42) Zhu, Z.-T.; Mason, J. T.; Dieckmann, R.; Malliaras, G. G. Humidity Sensors Based on Pentacene Thin-Film Transistors. *Appl. Phys. Lett.* **2002**, *81*, 4643−4645.
(43) Goldmann, C.; Gundlach, D. J.; Batlogg, B. Evidence of Water-Related Discrete Trap State Formation in Pentacene Single-Crystal Field-Effect Transistors. *Appl. Phys. Lett.* **2006**, *88*, 063501.
(44) Li, D.; Borkent, E.-J.; Nortrup, R.; Moon, H.; Katz, H.; Bao, Z. Humidity Effect on Electrical Performance of Organic Thin-Film Transistors. *Appl. Phys. Lett.* **2005**, *86*, 042105.